# Assessment of vertical air motion among reanalyses and qualitative comparison with VHF radar measurements over the two tropical stations

*K. N. Uma[1], Siddarth Shankar Das[1], M. Venkat Ratnam[2], and K. V. Suneeth[1]*

[1]Space Physics Laboratory, Vikram Sarabhai Space Centre, ISRO, Trivandrum-695022, India
[2]National Atmospheric Research Laboratory, Dept. of Space, Gadanki-517112, India

*e-mail : urmi_nmrf@yahoo.com

**Abstract**

Vertical wind (*w*) is one of the most important meteorological parameters for understanding a range of different atmospheric phenomena. Very few direct measurements of *w* are available so that most of the time one must depend on reanalysis products. In the present study, assessment of *w* among selected reanalyses, (ERAi, ERA5, MERRA-2, NCEP/DOE-2 and JRA-55) and qualitative comparison of those datasets with VHF radar measurements over the convectively active regions Gadanki (13.5°N and 79.2°E) and Kototabang (0°S and 100.2°E) are presented for the first time. The magnitude of *w* derived from reanalyses is 10-50% less than that from the radar observations. Radar measurements of *w* show downdrafts below 8 to 10 km and updrafts above 8-10 km over both locations. Inter-comparison between the ensemble of reanalyses with respect to individual reanalysis shows that ERAi, MERRA-2 and JRA-55 compares well with the ensemble compared to ERA5 and NCEP/DOE-2. There is no significant improvement in the *w* due to the effect of different spatial sampling. Directional tendency shows that the percentage of updrafts captured is reasonably good, but downdrafts are not well captured by all reanalyses. Thus, caution is advised when using vertical velocities from reanalyses.

Key Words: Vertical velocity, MST Radar, Equatorial Atmosphere Radar, Reanalysis

## 1 Introduction

Vertical air motion (*w*) in any region of the Earth's atmosphere reflects the structure and dynamical features of that region. Importantly, in the lower part of the atmosphere, sudden widespread changes in the weather are usually associated with variations in vertical air motion. The magnitude of *w* is a factor of ten or more smaller than the horizontal wind; nevertheless, it is crucial in the evolution of severe weather (*Peterson and Balsley*, 1979). Adiabatic cooling associated with upward motion leads to the formation of clouds and precipitation and adiabatic warming associated with downward motion leads to the dissipation of clouds. In addition, subsidence leads to adiabatic warming, which results in the formation of stable inversion layers. Extensive studies have been done on the relationships between *w* and precipitation/convection over the tropics (*Back and Bretherton*, 2009; *Uma and Rao*, 2009a; *Rao et al*., 2009; *Uma et al*., 2011 and references therein). Thus, *w* plays a vital role in day-to-day changes in the weather. Different scales of variability exist in *w* ranging from microscale to meso synoptic, and planetary - scales (*Uma and Rao*, 2009b). It also controls energy and mass transport between the upper troposphere and lower stratosphere (*Yamamoto et al*., 2007, *Rao et al*., 2008). In a nutshell, knowledge of *w* is helpful for evaluating virtually all physical processes in the atmosphere. Hence precise measurements of *w* could serve a guiding factor for studying many processes in the atmosphere.

The small magnitudes of *w* make it very difficult to measure, as the errors involved in measurements often exceed the actual values. Direct and indirect methods exist to measure *w* (e.g. Doppler measurements using radars for profiling, sonic anemometers in the boundary layer and also aircrafts) as well as indirect computational methods (e.g., adiabatic, kinematic and quasi-geostrophic vorticity/omega methods). Remote sensing measurements of *w* are thus restricted to locations where radars are situated. Using aircrafts *Schumann*, (2019) studied the relationships between horizontal kinetic energy spectra of vertical wind and horizontal divergence of the divergent horizontal wind components, by separating it from the rotational wind components by known Helmholtz decomposition methods. In general, $w$ is derived diagnostically from horizontal winds and temperatures, which is an indirect estimation. This estimation gives a general view on the distribution of ascending and descending motion on the synoptic-scale within the quasi-geostrophic framework (*Tanaka and Yatagai*, 2000; *Rao et al.*, 2003).

Reanalyses evaluate the vertical pressure velocity (omega) using indirect estimation (e.g., *Dee et al.*, 2011). Any reanalyses products assimilate as much as $10^7$ observations per day, which is inclusive of both conventional (radiosonde, tower, aircrafts, wind profilers (wherever possible), etc.) as well as various satellite observations. However, reanalyses combine both observations and model outputs to produce systematic variation in the atmospheric state (e.g., *Fujiwara et al.*, 2017). It is to be noted that the vertical velocity provided by any reanalysis data center is estimated indirectly from the horizontal wind components and temperature, which itself has mismatch among various reanalyses data (e.g., *Das et al*., 2016; *Kawatani et al.*, 2016). Thus, this can possibly induce the discrepancy in the estimated vertical velocity among various reanalyses. For example, in the kinematic method, omega is estimated by integrating the mass continuity equation assuming inviscid adiabatic flow. However, this kinematic estimate suffers from uncertainties in the observations as omega is estimated from horizontal divergence (*Tanaka and Yatagai*, 2000). This source of uncertainty is particularly important for reanalyses, where assimilation increments in horizontal winds may be comparable to the uncertainty. A 10% error in the wind may lead to a 100% error in the estimated divergence (*Holton*, 2004). Omega from the thermodynamic energy equation is less sensitive to horizontal winds as it mainly depends on the temperature gradient. However, in this method the local rate of change in temperature must be measured accurately, meaning that observations must be taken at frequent intervals in time to estimate $\partial T / \partial t$ accurately (*Holton*, 2004). This methodology fails in areas of strong diabatic heating, especially where condensation and evaporation are involved. The quasi-geostrophic method for estimating omega neglects ageostrophic effects, friction and diabatic heating (*Stepanyuk et al.*, 2017). It is to be noted from the above discussions that calculating *w* from indirect estimation has more uncertainties. Hence reanalyses that use indirect estimation, involve underlying approximations and assimilations and are not error-free (*Kennedy et al*., 2012).

Other indirect methods can be used to derive *w* from radar measurements in the middle and upper atmosphere, where direct measurements of vertical wind are not possible due to technical constraints. These methods include Doppler weather radar, Medium Frequency (MF) radar and meteor radar. Doppler weather radar uses an indirect method to calculate vertical winds (*Liou and Chang*, 2009; *Matejka*, 2002). Meteor radar also cannot determine vertical velocity directly as the winds are determined from meteor showers using a wide beamwidth. As a consequence, *Laskar et al*. (2017) calculated vertical wind from meteor wind radar data based on a "Kinematic" method using the continuity equation and hydrostatic balance. *Dowdy et al.* (2001) have calculated vertical wind using the horizontal momentum and mass continuity equations from the MF radar data. However, indirect methods are only adopted when direct methods cannot be used.

Very-high frequency (VHF) and ultra-high frequency (UHF) vertical pointing radars are the most powerful tools for determining vertical air motion (velocity) with high temporal and vertical resolution. However, the magnitude may still not be directly comparable between reanalysis products and observations as the reanalyses provide the intensity of vertical air motion over wide areas (> 25 $km^2$), whereas the radar measurements provide information for a narrower column over a single location. Thus, the best way to assess reanalysis estimates of *w* against radar measurements is to compare its directional tendencies. A number of studies have evaluated vertical motion across reanalyses (in the context of trajectories, wave activity, large-scale motion, etc.), so the primary novelty of this work is the evaluation against radar observations. The present study focuses on the assessment of *w* among various reanalyses using VHF radar measurements from two tropical stations where the convective activity is frequent: Gadanki and Kototabang. Evaluations of this type are critically important as reanalyses estimates of *w* are widely used by the scientific community to understand and simulate a variety of atmospheric processes. In section 2, the data and methodology are described. Section 3 provides results and discussion followed by summary and concluding remarks in section 4.

## 2 Data and Methodology

### *2.1 Radar measurements*

Remote sensing measurements of *w* are obtained from the Indian Mesosphere-Stratosphere-Troposphere Radar (IMSTR) located at Gadanki ($13.5^{o}$N and $79.2^{o}$E) and the Equatorial Atmosphere Radar (EAR) located at Kototabang ($0.2^{o}$S and $100.2^{o}$E). Figure 1a and 1b show the topography map of the location of both the radars, i.e. Gadanki and Kototabang respectively, generated by using the Shuttle Radar Topography Mission (SRTM) data (*Farr et al.*, 2007). Gadanki is located in the southern peninsula of tropical India, about 90 km off the east coast and it is surrounded by hills. Kototabang is located in the western part of Sumatra Island and EAR is situated in the mountainous region with the highest peak of about 2 km. Both the IMSTR and EAR are pulsed coherent radars operating at 53 MHz and 47 MHz, respectively. These instruments are used to estimate *w* by measuring the Doppler shift in the vertical beam. The technical details and operational parameters of the IMSTR have been given by *Rao et al*. (1995) while those for the EAR have been given by *Fukao et al*. (2003). Both the radars specifications and parameters used for the present measurements are listed in Table 1.

In the present study measurements of $w$ from VHF radars are used to assess vertical motion between the surface and the lower stratosphere. Data collected from the IMSTR between 17:30 and 18:30 LT (LT=GMT+5:30 hr) from 1995 to 2015 are analyzed using the adaptive method (*Anandan et al*., 2001). This is the common operational mode of the IMSTR for deriving the winds and represents the only data available for such a long period of time. In general, 4-8 vertical profiles are averaged to create daily mean profiles. Averaging is conducted using the arithmetic mean as it represents the central tendency, which is generally used for wind averaging. In a vertically pointing beam, signal-to-noise ratio (SNR) decreases with height except in stable layers (like the tropopause) and in the presence of strong turbulence. Above 25 km, the SNR becomes constant in the absence of atmospheric signals. Data in this region can be therefore treated as noise and used to estimate the threshold SNR (*Uma and Rao*, 2009b). Noise levels estimated in this way lie between -17 dB and -19 dB with a 2$\sigma$ value of 3 dB (where $\sigma$ is the standard deviation). Thus data having SNR less than -15 dB are discarded from the present analysis. Data from intense convective days (checked for individual profiles), defined as $w$ being less/greater than ± 1 ms$^{-1}$ are also discarded as these data severely bias the climatological mean vertical velocity (e.g. *Uma and Rao*, 2009b). The data discarded is less than 1 % of the total data. Quality control metadata for the EAR measurements are available online (http://www.rish.kyoto-u.ac.jp/ear/data/index.html). The EAR operates continuously and this study uses hourly data (diurnal data of single day) from 2001 to 2015. The EAR data during convective periods are eliminated following the same criteria as for the IMSTR, a second screening step. Each full diurnal cycle (after removing convective profiles) is averaged and considered as a single daily profile for the EAR. For both radars, vertical velocity (cm s$^{-1}$) is directly estimated using equation (1)

$$w = -\frac{\lambda}{2} f_d, \tag{1}$$

where $\lambda$ is the radar wavelength (in cm) and $f_d$ is the Doppler velocity (Hz).

It is known that estimates of *w* derived from VHF radar measurements are vulnerable to biases due to tilting layers, strong horizontal winds (e.g., jet-stream), complex topography, Kelvin-Helmholtz instabilities and gravity waves (*Rao et al.*, 2008 and references therein). *Rao et al*. (2008) has discussed in detail the biases that can cause spurious diagnosis of downward wind as proposed by *Nastrom and VanZandt* (1994). In addition, they have also discussed the potential biases caused by beam pointing errors as mentioned by *Hauman and Balsley* (1996) and have conducted critical analysis to rule out beam pointing biases from VHF radar data. It is also to be noted that the topography over the two locations can generate mountain waves if strong low-level winds are prevailing. Strong low-level winds are prevalent over Gadanki only from June to August and during these months, there is a critical level existing between 6 and 7 km due to the presence of strong wind shear, which will not support the propagation of mountain waves to higher altitudes. This wind shear exists throughout the year over Kototabang. Hence the effect of mountain waves will be minimal over both these locations on vertical velocity. As proposed by *Nastrom and VanZandt* (1994) on the bias caused by gravity waves, *Rao et al*. (2008) have investigated biases caused by gravity waves by calculating the variances and found that downward wind measurements below 10 km are essentially unaffected by gravity waves. Their analysis clearly showed that the mean downward motion below 10 km and upward motion above 10 km are real and not caused by measurement biases, and also that the known biases do not change the direction of the background *w* when measurements are averaged over longer periods of 10 years.

### 2.2 *ERA-Interim (ERAi)*

ERAi is global reanalyses data which is developed by European Centre for Medium-Range Weather Forecasts (ECMWF). The data assimilation scheme used is 4D-Var of the upper-air atmospheric state and have effectively anchored both satellite and in-situ observations. This scheme updates parameters that define bias corrections required for satellite observations. The model has improved in the representation of moist physical processes. Advances have also been made with respect to soil hydrology and snow in land surface models. The detail of the model is given in (*Dee et al.,* 2011). We use 6-hourly vertical velocities from the ECMWF Interim reanalysis (ERAi) from 1995 to 2015. The grid resolution of ERAi is 0.75$^o$ (latitude) x 0.75$^o$ (longitude). The nearest grid points are taken for Gadanki (13.68$^o$N, 79.45$^o$E) and Kototabang (0.35$^o$S, 100.54$^o$E). Although 37 pressure levels up to 1 hPa resolution are available, we have restricted the dataset to 21 km, which is about 50 hPa, as that is the maximum radar range.

### 2.3 *ERA5*

ERA fifth-generation (ERA5) is the atmospheric reanalysis produced by ECMWF. It is an improved version of ERAi. The data assimilation scheme used is 4D-Var and it assimilates the NCEP stage IV quantitative precipitation estimates produced over the USA by combining precipitation estimates from the Next-Generation Radar (NEXRAD) network with gauge measurements. The moist physics scheme is improved by including freezing rain. The long wave radiation scheme is modified in ERA5. The evolution of the top soil layer, snow and sea ice temperatures are included. It uses observations from various satellites which include upper air temperature, humidity and ozone. It also used bending angles from GNSS. It provides much higher spatial (30 km) and temporal resolution (hourly) from the surface up to 80 km (137 levels). ERA5 also features much improved representation especially over the tropical regions of the troposphere and better global balance of precipitation and evaporation. Many new data types not assimilated in ERAi are ingested in ERA5 (*Hoffmann et al.*, 2019). The grid resolution of ERA5 is 0.28$^o$ (latitude) x 0.28$^o$ (longitude). The details are available in (Hersbach et al., 2020). We have taken hourly data from ERA5. The nearest grid points are again taken for Gadanki (13.63$^o$N, 79.31$^o$E) and Kototabang (0.14$^o$S, 100.40$^o$E), and the data period is 2002-2015.

## 2.4 *MERRA-2*

The Modern-Era Retrospective analysis for Research and Applications, version 2 (MERRA-2) is the latest reanalysis of the modern satellite era produced by the National Aeronautics and Space Administration's (NASA) Global Modelling and Assimilation Office (GMAO). The scheme used in MERRA-2 is an improved version of MERRA. It uses a three-dimensional variational (3D-Var) algorithm based on the grid point statistical interpolation and also uses an incremental analysis update. It assimilates bending angle observations, satellite radiances from both polar as well as geostationary infra-red and microwave sounders. In addition it also assimilates water vapor and ozone. MERRA-2 includes aerosol analysis and provide data for 42 pressure levels from the surface to 0.01 hPa with a temporal resolution of 3 h and horizontal resolution of 0.5$^o$ (latitude)x 0.625$^o$ (longitude). We used MERRA-2 Assimilation (ASM) data. Details have been provided by *Gelaro et al.* (2017). The nearest grid points are used for Gadanki (13.5$^o$N, 79.37$^o$E) and Kototabang (0.14$^o$S, 100.00$^o$E), with data spanning from 1995 to 2015.

## 2.5 *NCEP/DOE-2*

The National Center for Atmospheric Research and Department of Energy (NCEP/DOE-2) reanalysis is an updated version of NCEP-1 by fixing the known processing errors in NCEP-1. The variational scheme used is 3D-Var and it provides more accurate pictures of soil wetness and near-surface temperature over land, the land surface hydrology budget, snow cover, and radiation fluxes over the ocean. It is based on the NCEP operational model with a horizontal resolution of 209 km and 28 vertical levels. The temporal coverage is four times per day. NCEP/DOE-2 products are improved relative to NCEP-1, having fixed errors and updated parameterizations of physical processes, as evaluated by *Kanamitsu et al.* (2002). The grid resolution of NCEP/DOE-2 is 2.5$^o$ (latitude) x 2.5$^o$ (longitude). The data for the present study covers  from 1995 to 2015 and is extracted at the nearest grid points to Gadanki (12.5$^o$N, 77.5$^o$E) and Kototabang (0, 100.00$^o$E).

## 2.6 *JRA-55*

The Japanese 55-year reanalysis  (JRA-55) is an updated version of the earlier JRA-25 with new data assimilation and prediction systems (*Kobayashi et al.*, 2015). New radiation schemes, higher spatial resolution and 4D-var data assimilation with variational bias correction for satellite radiances have been used to generate the JRA-55 products. This reanalysis includes variation in greenhouse gas concentrations with time, as well as the new representations of land surface parameters, aerosols, ozone and sea surface temperature. The grid resolution of JRA-55 is 1.25$^o$ (latitude) x 1.25$^o$ (longitude). The nearest grid points are taken for Gadanki (13.75$^o$N, 78.75$^o$E) and Kototabang (0, 100$^o$E) and the data period is 1995-2015.

For all the reanalyses data, *w* (in cm s$^{-1}$) is estimated using the formula :

$$w = -\frac{1}{g}\omega\frac{RT}{p} \qquad (2)$$

where $\omega$ is the vertical velocity in pressure coordinates (in Pa s$^{-1}$), T is the absolute temperature (K), p is the atmospheric pressure (hPa) and R (=287 J kg$^{-1}$ K$^{-1}$) is the gas constant for dry air. To compare measured vertical wind with the reanalysis products, we take the reanalysis data corresponding to 12 GMT for Gadanki and the daily mean for Kototabang. The details of the schemes used in reanalysis are provided in Table 2.

# 3 Results and Discussion

Figure 2 shows the inter-comparision of layer averaged daily *w* measured from IMSTR with different reanalyses (ERAi, ERA5, MERRA-2, NCEP/DOE-2, and JRA-55) over Gadanki for (a) January 2007, and (b) August 2007.   Both radar and all the reanalyses data sets are taken at 12 UTC, and the month and year are chosen in such a way to have maximum days of radar observations in two different seasons (winter and summer).

Similarly, EAR observation is also compared with different reanalysis data but for January 2008 and August 2008 as shown in Fig.3. However, both EAR and reanalysis data are diurnal averaged (24 hrs). It is observed that the magnitude of *w* measured from radar observations is an order higher than the reanalysis data over both the locations (Gadanki and Kototabang). Most of the time, reanalysis data are comparable in direction with radar observations, whenever updrafts are observed. It is also observed that there is mismatch between the *w* estimated in the different reanalyses. *Gage et al.* (1992) described that by averaging radar data for a long-period of time can give a better measurement of *w* in clear-air condition and thus in this context, we have taken long-term averaging.

Figure 4 shows the climatological monthly mean altitude profile of *w* obtained from the IMSTR (observations) and the ERAi, ERA5, MERRA-2, NCEP/DOE-2 and JRA-55 reanalysis data over Gadanki. Although the magnitudes are of the same order between the observations and reanalyses, significant differences are identified in the figures. Convective days are discarded from the radar data (observations) as mentioned in the previous section and those days are also eliminated from all reanalysis data sets. The quantitative differences may be attributed to the spatial averaging implicit in the reanalyses products, whereas the radar measurements are for a single point. Thus we only discuss the tendency of *w* as it is used to represent the variation of *w*, rather than its magnitude. The IMSTR observations show updrafts between 8 and 20 km from December to April, with the largest values in the tropical tropopause layer (TTL, 12-16 km), These features are not reproduced by any of the reanalyses, which all show downdrafts from December to April between 1 km and the tropopause level (mean tropopause is ~ 16.5 km). By comparison, downdrafts are observed in the IMSTR below 6 km in April, which may be attributed to pre-monsoon (March-May) precipitation and evaporation (*Uma and Rao*, 2009a). Vertical velocity in ERAi differs in both magnitude and direction from other reanalyses, especially in the lower troposphere from

March to June. Meanwhile, the magnitude of vertical velocity in ERA5 is a little larger than that in the other reanalyses from May to June. Updrafts are observed in the TTL by the IMSTR during June, when all reanalyses show similar features but only located below the TTL. During July and August both the radar observations and the reanalyses show updrafts in the vicinity of the TTL. Updrafts are observed in the TTL from September to November but the peak in the updrafts is shifted lower than that observed by the IMSTR. Below 8 km, the IMSTR shows downdrafts from April to October. The reanalyses data are unable to reproduce downdrafts above 2 km.

We have also analyzed *w* from the EAR (Kototabang) where the observations are available for the full diurnal cycle (measurements of hourly averages for 24 hrs of observations). All reanalyses data over Kototabang are averaged for the full diurnal cycle. Figure 5 shows the monthly mean climatology of daily mean *w* from the EAR observations and the five reanalyses over Kototabang. All the reanalyses agree well with each other over Kototabang. The updrafts in the TTL are well reproduced by all five reanalyses although the magnitude and vertical location of the maximum in *w* remain lower than observed. However none of the reanalyses reproduces the downdrafts. A distinct bimodal distribution in *w* from May to September (two peaks between 8-10 km and 14-17 km) with a local minimum between 12 and 13 km is observed in the EAR measurements which is not observed in the reanalysis. The magnitudes of both updrafts and downdrafts are larger than those observed over Gadanki. JRA-55 produces the largest *w* among the reanalyses. The monthly means show significant differences in the direction of *w* between the observations and the reanalyses below 6 km.

*Gage et al.* (1992) studied the long-term diurnal variability of *w* at Christmas Island ($2^{o}$N) and found the *w* varies between ±4 cm $s^{-1}$. The observations showed updrafts below 4 km, downdrafts between 4-14 km and updrafts above 12 km. *Gage et al.* (1991) have explained that the downward motion in the troposphere is consistent with a heat balance in the clear-air between adiabatic warming of descending air and radiative cooling to space. The ascending motion in the upper troposphere and lower stratosphere is due to large diabatic heating caused by ice particle in the cirrus. *Rao et al.* (2008) have shown the long-term mean of *w* over Gadanki and Kototabang and found *w* varies between -0.3 to +0.6 cm $s^{-1}$. The authors observed downdrafts below 6 km and updrafts above it in all the seasons. The mean pattern of *w* profile observed by radars over all the tropical sites (i.e. Christmas Island, Gadanki and Kototabang ) show similar characteristics and explain that the vertical transport of air from the troposphere to the lower stratosphere is a two-step process as discussed by *Rao et al.* (2008). *Uma and Rao* (2009b) have reported the diurnal variation of *w* in different seasons, although their observations had only 1-2 diurnal cycles per month over Gadanki. They found significant variations in the seasonal variability of diurnal cycle as large as ±6 cm $s^{-1}$ over Gadanki using IMSTR. The present observations are limited to 16:30 to 17:30 IST, with all reanalyses data over Gadanki taken at 12 UTC (17:30 IST). Thus, time-averaged climatological mean biases can be neglected.

To establish the robustness of the results we have used different averaging procedures to assess the consistency of the variability in *w* at monthly scales. Monthly mean climatological profiles of *w* from radar observations and various reanalyses over Gadanki and Kototabang are shown in Figure S1 (supplementary). Downdrafts in the troposphere are not captured by any of the reanalyses over either location. By contrast, updrafts in the TTL are generally reproduced in the monthly mean, though their magnitudes are often underestimated by the reanalyses. ERAi underestimates the magnitude of both updrafts and downdrafts over Gadanki, while NCEP/DOE-2 underestimates the magnitude of updrafts over Kototabang.

Monthly means calculated over five-year periods from both the radar data and ERAi are shown in Figure 6 for Gadanki and Figure 7 for Kototabang. The reanalysis shows similar behavior to the overall climatology in each five-year average. The overall patterns of updrafts and downdrafts in the radar measurements of vertical velocity are also similar, indicating a consistent performance of the radar over the full 20 year analysis period.

To further elucidate potential biases in the results due to averaging, we have taken ERA5 at 12 UTC and compared it to the daily mean (obtained by averaging *w* at different times of the day) to show that the sampling restrictions at Gadanki do not bias the results obtained. Figures 8 and 9 show the mean *w* obtained at 12 UTC and also the mean obtained by averaging hourly analyses for each day for Gadanki and Kototabang, respectively. ERA5 is chosen for this evaluation as the data are available at one-hour intervals. The analysis shows some differences in the magnitude of *w*, with 12 UTC generally showing larger magnitudes compared to the daily means over Gadanki (although no such systematic differences are observed in Kototabang). The directional tendencies are also similar in both the profiles at both locations. This analysis shows that the results are not biased by taking data only at 12 UTC over Gadanki.

Our analysis to this point shows the level of consistency between the features observed by the radar and those in the reanalysis. To further understand the relative differences among the reanalyses we perform a monthly mean comparative analysis among the reanalyses, as shown in Figures 10 and 11 for Gadanki and Kototabang, respectively. We take an ensemble mean of all the five reanalyses and then subtracted the ensemble mean from each reanalysis. The differences are less than ±0.5 cm $s^{-1}$ during December-January-February (DJF, winter),. During MAM, the difference between the ensemble and reanalysis show ±2 cm $s^{-1}$ below 5 km. Below 5 km NCEP/DOE-2 and ERAi is less, whereas ERA5, Merra-2 and JRA-55 are more than the ensemble. The difference above 6 km is less than ±0.5 cm $s^{-1}$ above 6 km. JRA-55 shows a good comparison with the ensemble and above 10 km all the reanalyses the differences are minimal with the ensemble. During the monsoon (JJA), the difference is comparatively high in June compared to July and August. NCEP/DOE-2 and ERA5 are more and other reanalyses are less than the ensemble, however during July and August NCEP/DOE-2 it is less in the upper troposphere (10-18 km). Merra-2 and ERAi shows a good comparison with respect to the ensemble during July and August, JRA-55 also shows a good comparison in addition to Merra-2 and ERAi. During SON, the differences are comparatively less than MAM and JJA. The difference is less than ±0.5 cm $s^{-1}$ during October and November except in September between 10 and 15 km where ERA5 and Merra-2 are more and ERAi and NCEP/DOE-2 are less than the ensemble. In general, ERA5 and NCEP/DOE-2 shows considerably more difference with the ensemble and other reanalyses (ERAi, Merra-2 and JRA-55) compare well with the ensemble.

Over Kototabang (Figure 11), it is interesting to note the difference between the ensemble and different reanalyses show a consistent pattern during all the months. JRA-55 and ERAi show good comparison with the ensemble, as the differences are less than ±0.2 cm $s^{-1}$ in all the seasons, except in November where it exceeds ±0.5 cm $s^{-1}$ in the lower and middle troposphere. Merra-2 is more and NCEP/DOE-2 is less than the ensemble at all the height regions. ERA5 is less below 10 km and more above with respect to the ensemble.

There may be some probable reasons for the differences in the vertical velocity measured by observations and those retrieved from reanalysis. The main bias in *w* might occur in the reanalysis due to the following (1) Indirect estimation of omega, (2) local topography influence in the reanalysis, (3) use of different schemes in the boundary layer, (4) interactions between subgrid physical parameterizations and the large-scale flow and (5) spatial and temporal sampling. However, it is difficult to address the above issues other than the spatial and temporal sampling. To elucidate the spatial-temporal averaging on the vertical velocity we have chosen different grid resolutions with Gadanki as a centroid and the map is shown in Fig. 12a. G1 to G5 represent different grid resolutions, varying from $0.7^o$ to $5^o$. The data chosen is for January and July 2007 from ERAi. The height profile of *w* at different grid resolution and time is shown in Fig. 12b for January and in Fig.12c for July. It is observed that the grid resolution does not have any influence on the *w*. However, a significant change is observed between 00 and 12 UTC in the month of January which affected the diurnal mean in *w* (shown in the last panel). The same is not reflected in the month of July. The result shows that the narrowing down the reanalysis data spatially (reducing the horizontal sampling) will not improve the retrieval of *w* in any reanalyses.

The direction of *w* is an essential metric for comparing the reanalysis with the observations. We therefore show the directional tendencies from the IMSTR and the EAR measurements relative to those from the reanalysis data. Figure 13a shows the directional tendencies based on the IMSTR and the reanalyses over Gadanki, while Figure 13b shows the directional tendencies based on the EAR and the reanalyses over Kototabang. The directional tendency is calculated at each height for every month when the radar or reanalysis data exceed 0.1 $cms^{-1}$ in either direction. The directional tendency for each month is estimated and then aggregated into seasons. These directional tendencies are given in terms of percentage of occurrence with respect to height. The tendency is calculated separately for updrafts and downdrafts.

Over Gadanki during DJF all reanalyses produce updrafts (simultaneously by both radar and reanalysis) less than 10% of the time throughout the profile. During MAM these ratios increase to around 15%, with NCEP/DOE-2 producing updrafts about 25% of the time. During JJA and SON, the percentage occurrence increases with the height from 25% to a maximum of 50% between 12 and 14 km. The percentage occurrence of updraft then decreases from 14 to 20 km. This tendency trend is similar for all reanalyses. The maximum ratio of updrafts over Gadanki is located between 12 and 15 km altitude. The percentage occurrence of downdrafts over Gadanki is also less than 50% at all levels. During DJF and

MAM the reanalyses produce downdrafts 40 to 50% of the time, a much higher frequency than that for updrafts (<10%). This fraction decreases above 10 km. By contrast, the percentage of downdrafts produced during JJA and SON is less than that of updrafts, with frequencies less than 25% at all levels during these seasons.

Over Kototabang the percentage occurrence of updrafts increases with height in all seasons reaching a maximum of 75- 90% between 10 and 14 km. Above 14 km the percentage decreases to a minimum of 5% at 19 km. Updrafts are rarely produced by the reanalyses altitudes less than 4 km. It is important to note that none of the reanalyses produce daily mean downdrafts exceeding 1 cm $s^{-1}$ except ERAi and ERA5 which produced downdrafts below 6 km. The percentage of downdrafts increases above 17 km where it reaches a maximum and show occurrence frequencies around 65 to 75% above 18 km.

## 4 Summary

The present study assesses the vertical motion (*w*) in reanalyses against radar observations from the convectively active regions Gadanki and Kototabang. The assessment is carried out for five different reanalyses: ERAi, ERA5, MERRA-2, NCEP/DOE-2 and JRA-55. Measurements were collected using VHF radar at both locations. We have used 20 years of data from Gadanki and 17 years of data from Kototabang. The following points summarize the results of this unique study

1. The magnitude of *w* obtained from reanalyses is underestimated by 10-50% relative to the radar observations.
2. Observations over Gadanki showed updrafts from 8 to 20 km year around. All the reanalyses only reproduced this feature during JJA and SON when magnitudes were larger than 0.5 cm $s^{-1}$ in the reanalyses data. However, the vertical location of the updrafts differs between the observations and the reanalyses. Downdrafts below 8 km are not captured well by reanalyses data.

3. Over Kototabang, all five reanalyses did not consistently reproduce downdrafts below 8 km in all months. Updrafts in the UTLS are captured well; however, the peak in the vertical distribution of *w* is different as over Gadanki.
4. Inter-comparison between the ensemble and each reanalysis data shows the ERAi, MERRA-2 and JRA-55 compares well with the ensemble compared to ERA5 and NCEP/DOE-2. Analysis also showed that the reduction in spatial sampling in any reanalysis does not have significant improvement in the magnitude *w*.
5. Assessment of directional tendencies show that updrafts are reproduced reasonably well in all five reanalyses data but downdrafts are not reproduced at all.

Our analysis reveals that downdrafts are not well captured in all the five reanalyses data. The location of the largest updrafts is also shifted lower in reanalyses than in the observations. Hence, reanalysis data should be used with care for representing various atmospheric motion calculations (*viz*. diabatic heating, convection, etc.) that mainly depend on the direction of *w*. This study provides the reanalysis community an initial basis to improve the methodology for calculating *w* in reanalysis, as this is a much sought-parameter for atmospheric circulation calculations and analysis.

**Acknowledgements**

Authors would like to acknowledge all the technical and scientific staffs of National Atmospheric Research Laboratory (NARL) and Research Institute of Sustainable Humanosphere (RISH), who directly or indirectly involved in the radar observations. Thanks to all the reanalyses data centres for providing the data through the portal of Research data archival (RDA) of NCEP/UCAR. One of the author KVS thank Indian Research Organisation for providing research associateship during this study. We sincerely thanks all the three referees, Executive Editor and Editor for their constructive comments and suggestions.

**Data availability:** Analysed data (both radars and reanalyses) used in this study can be obtained on request. Raw time series data are available through open access in the following websites:

For Indian MST Radar : www.narl.gov.in

For EAR radar : www.rish-kyoto-u.ac.jp/ear/index-e.html

ERAi, ERA5, JRA-55 and NCEP/DOE-2 were downloaded from https://rda.ucar.edu and MERRA-2 from https://disc.gsfc.nasa.gov.in

**Author's Contributions**

KNU conceived the idea for validation of vertical velocity among the reanalyses. SSD, MVR, and KVS collected and analysed the MST radar spectrum data. All the authors contribute for generation of figures, interpretation and manuscript preparation. The data used in the present study can be obtained on request.

**Conflict of Interest**

The authors declare that there is no conflict of interest.

## References


Anandan, V.K., Reddy, G.R., Rao, P.B.: Spectral analysis of atmospheric signal using higher orders spectral estimation technique, IEEE Trans. Geosci. Remote Sens., 39, 1890. https://doi.org/10.1109/36.951079, 2001.

Arakawa, A. and Schubert, W.H.: Interaction of a cumulus cloud ensemble with the large-scale environment- Part I, J. Atmos. Sci., 31(3), 674-701, https://doi.10.1175/1520-0469 031<0674:IOACCE>2.0.CO;2, 1974.

Back, L. E., and Bretherton C.S.: Geographic variability in the export of moiststatic energy and vertical motion profiles in the tropical Pacific, Geophys. Res. Lett., 33, L17810, https://doi.org/10.1029/2006GL026672, 2006.

Bechtold, P., Chaboureau, J.P., Beljaars, A., Betts, A.K., Köhler, M., Miller, M. and Redelsperger, J.L.: The simulation of the diurnal cycle of convective precipitation over land in a global model. Q. J. Roy. Met. Soc., 130 (604), pp.3119-3137, https://doi.org/10.1256/qj.03.103, 2004.

Bechtold, P., Koehler, M., Jung, T., Doblas- Reyes, F., Leutbecher, M., Rodwell, M.J., Vitart, F., and Balsamo, G.: Advances in simulating atmospheric variability with the ECMWF model: From synoptic to decadal time- scales, Q. J. Roy. Met. Soc., 134 (634), pp.1337-1351, https://doi. 10.1002/qj.289,2008.

Briegle, B. P.: Longwave band model for thermal radiation in climate studies, J. Geophys. Res., 97, 11475-11485, https://doi.org/10.1029/92JD00806, 1992 .

Campana, K. A., Hou, Y.T., Mitchell, K. E., Yang, S. K., and Cullather, R.: Improved diagnostic cloud parameterization in NMC's global model. Preprints, 10th Conf. on Numerical Weather Prediction, Portland, OR, Amer. Meteor. Soc., 324-325, 1994.

Chou, M.D.: A solar radiation model for use in climate studies., J Atmos.Sci., 49, 762-772, https://doi.org/10.1175/1520-0469(1992)049<0762:ASRMFU>2.0.CO;2, 1992.

Chou, M. D., and Lee, K. T.: Parameterizations for the absorption of solar radiation by water vapor and ozone, J. Atmos. Sci., 53, 1203-1208, https://doi.10.1175/1520-0469(1996)053<1203:PFTAOS>2.0.CO;2, 1996.

Chou, M.D., and Suarez, M.J.: A Solar Radiation Parameterization (CLIRAD-SW) Developed at Goddard Climate and Radiation Branch for Atmospheric Studies. NASA Technical Memorandum NASA/TM-1999-104606, 1999.

Chou, M.D., Lee, K. T., and Yang, P.: Parameterization of shortwave cloud optical properties for a mixtureof ice particle habits for use in atmospheric models, J. Geophys. Res., 107, 1-9, https//doi:10.1029/2002JD002061, 2001.

Das, S. S., Uma, K. N., Bineesha, V. N., Suneeth, K. V., G. Ramkumar G.: Four decadal climatological intercomparison of rocketsonde and radiosonde with different reanalysis data: results from Thumba Equatorial Station, Q. J. Roy. Met. Soc., https://doi.org/ 10.1002/qj.2632, 2015.

Dee D. P et al.: The ERA-Interim reanalysis: Configuration and performance of the data assimilation system, Q. J. R. Meteorol. Soc., 137, 553–597, https://doi.org/10.1002/qj.828, 2011.

Dowdy, A., R. A. Vincent, K. Igarashi, Y. Murayama and D.J. Murphy.: A comparison of mean winds and gravity wave activity in the northern and southern polar MLT. Geophy.Res.Lett., 28( 8), 1475- 1478. https://doi.org/10.1029/2000GL012576, 2001

European Centre for Medium-Range Weather Forecasts. 2009, updated monthly. ERA-Interim Project. Research Data Archive at the National Center for Atmospheric Research, Computational and Information Systems Laboratory. https://doi.org/10.5065/D6CR5RD9. Accessed 17 July 2019 and 29 July 2020.

European Centre for Medium-Range Weather Forecasts. 2017, updated monthly. ERA5 Reanalysis. Research Data Archive at the National Center for Atmospheric Research, Computational and Information Systems Laboratory. https://doi.org/10.5065/D6X34W69. Accessed 24 Jun 2019 and 30 July 2020.

Farr, T. G., Rosen, P. A., Caro, E., Crippen, R., et al. : The shuttle radar topography mission, Rev. Geophys., 45(2), http://dx.doi.org/10.1029/2005RG000183, 2007.

Fouquart,Y., Buriez, J. C., Herman, M., Kandel, R. S.: The influence of clouds on radiation: A climate-modeling perspective, J. Geophys. Res., 28,145-166, https:// doi.org/10.1029/RG028i002p00145, 1990.

Fukao, S., H. Hashiguchi, M. Yamamoto, T. Tsuda, T. Nakamura, M. K. Yamamoto, T. Sato, M. Hagio, and Y. Yabugaki.: Equatorial Atmosphere Radar (EAR): System description and first results, Radio Sci., 38(3), 1053, https://doi.org/10.1029/2002RS002767, 2003.

Fujiwara, M., Wright, J. S., Manney, G. L., et al.: Introduction to the SPARC Reanalysis Intercomparison Project (S-RIP) and overview of the reanalysis systems, Atmos. Chem. Phys., 17, 1417–1452, https://doi.org/10.5194/acp-17-1417-2017, 2017.

Gage, K. S., McAfee, J. R., Collins, W. G., Söderman, D., Böttger, H., Radford, A., & Balsley, B.: A comparison of winds observed at Christmas Island using a wind-profiling Doppler radar with NMC and ECMWF analyses, Bull. Amer. Meteor. Soc. (1988) 69 (9): 1041–1046,

https://doi.org/10.1175/1520-0477(1988)069<1041:ACOWOA>2.0.CO;2, 1988.

Gage, K. S., McAfee, J. R., Carter, D. A., Ecklund, W. L., Riddle, A. C., Reid, G. C., & Balsley, B. B.: Long-term mean vertical motion over the tropical Pacific: Wind-profiling Doppler radar measurements. Science, 254(5039), 1771-1773, https://doi.org/10.1126/science.254.5039.1771, 1991

Gage, K. S., McAfee, J. R., & Reid, G. C. (1992). Diurnal variation in vertical motion over the central equatorial Pacific from VHF wind-profiling Doppler radar observations at Christmas Island (2° N, 157° W). Geophysical research letters, 19(18), 1827-1830,https://doi.org/10.1029/92GL02105, 1992

Gelaro, et al.: The Modern-Era Retrospective Analysis for Research and Applications, Version 2 (MERRA-2), J. Clim., 30, 5419-5454, https://doi.org/10.1175/JCLI-D-16-0758.1, 2017.

Hersbach, H. et al.: The ERA5 global reanalysis. Q. J. Roy. Met. Soc., https://doi.org/10.1002/qj.3803

Holton, J.R.: An Introduction to Dynamic Meteorology, Academic Press, 3rd Ed, ISBN:9780123543554, 2004.

Hoffmann, L., Günther, G., Li, D., Stein, O., Wu, X., Griessbach, S., Heng, Y., Konopka, P., Müller, R., Vogel, B., and Wright, J. S.: From ERA-Interim to ERA5: the considerable impact of ECMWF's next-generation reanalysis on Lagrangian transport simulations, Atmos. Chem. Phys., 19, 3097–3124, https://doi.org/10.5194/acp-19-3097-2019, 2019.

Huaman, M., and B. B. Balsley.: Long-term average vertical motions observed by VHF wind profilers: The effect of slight antenna pointing inaccuracies, J. Atmos. Oceanic Technol., 13, 560– 569, 1996.

Iacono, M.J., Delamere, J. S., Mlawer, E. J., Shephard, M.W., Clough, S. A., and Collins, W.D.: Radiative forcing by long-lived greenhouse gases: Calculations with the AER radiative transfer models, J. Geophys. Res., 113, 1-8, https://doi.org/10.1029/2008JD009944, 2008.

Japan Meteorological Agency/Japan. 2013, updated monthly. JRA-55: Japanese 55-year Reanalysis, Daily 3-Hourly and 6-Hourly Data. Research Data Archive at the National

Center for Atmospheric Research, Computational and Information Systems Laboratory. https://doi.org/10.5065/D6HH6H41. Accessed 18 Jun 2019.

Kanamitsu M, W. Ebisuzaki, J. Woollen, S. K. Yang, J. J. Hnilo, M. Fiorino, G. L. Potter.: NCEP-DOE AMIP-II reanalysis (R-2). Bull. Am. Meteorol. Soc., 83: 1631–1643, https://doi.org/ 10.1175/BAMS-83-11-1631, 2002.

Kawai, H., and Inoue. T.: A Simple Parameterization Scheme for Subtropical Marine Stratocumulus, SOLA.,2,017-020,https://doi:10.2151/sola.2006-005, 2006.

Kawatani, Y., Hamilton, K., Miyazaki, K., Fujiwara, M., and Anstey, J. A.: Representation of the tropical stratospheric zonal wind in global atmospheric reanalyses, Atmos. Chem. Phys., 16, 6681-6699, doi: 10.5194/acp-16-6681-2016, 2016.

Kennedy, A. D., X. dong and B. Xi.: Comparison of MERRA and NARR Reanalyses with the DOE ARM SGP Data, J. Clim., https://doi.org/10.1175/2011JCLI3978.1, 2012.

Kobayashi, S., et al.: The JRA-55 Reanalysis: General specifications and basic characteristics, J. Meteorol. Soc. Jp., 93, https://doi.org/10.2151/jmsj.2015-001, 2015.

Laskar, F. I., et al.: Experimental evidence of arctic summer mesospheric upwelling and its connection to cold summer mesopause, Geophys. Res. Lett., 44, 9151- 9158. https://doi.org/10.1002/2017GL074759, 2017

Liou, Y.C., and Chang., Y. J.: A Variational Multiple-Doppler Radar Three-Dimensional Wind Synthesis Method and Its Impacts on Thermodynamic Retrieval, Mon. Wea. Rev., 137:11, 3992- 4010, https://doi.org/10.1175/2009MWR2980.1, 2009.

Matejka, T.: Estimating the most steady frame of reference from Doppler radar data, J. Atmos. Oceanic Technol., 19, 1035-1048, 2002.

Mlawer, E. J., Steven J.T., Patrick D.B., Michael J.I., and Clough. S. A.: Radiative transfer for inhomogeneous atmospheres: RRTM, a validated correlated-k model for the longwave, J. Geophys. Res., 102, 16663-16682, https://doi.org/10.1029/97JD00237, 1997.

Modern-Era Retrospective Analysis for Research and Applications, Version 2 (MERRA-2). ). Research Data Archive at the NASA Goddard Earth Sciences data and information service centre (GES-DISC) .http://dx.doi.org/10.5067/QBZ6MG944HW0 Accessed 5 Jul 2019.

Molod, A., Takacs, L., Suarez, M., and Bacmeister, J.: Development of the GEOS-5 atmospheric general circulation model: evolution from MERRA to MERRA2, Geosci. Model Dev., 8, 1339-1356, https://doi:10.5194/gmd-8-1339-2015, 2015.

Moorthi, S., and Suarez, M.J.: Relaxed Arakawa-Schubert. A Parameterization of Moist Convection for General Circulation Models, Mon. Wea. Rev., 120 (6): 978–1002, https://doi.org/10.1175/1520-0493(1992)120<0978:RASAPO>2.0.CO;2, 1992.

Morcrette, J. J.: Radiation and cloud radiative properties in the European Centre for Medium Range Weather Forecasts forecasting system, J. Geophys. Res., 96, 9121-9132, https://doi.org/10.1029/89JD01597, 1991.

Nastrom, G. D., and T. E. VanZandt.: Mean vertical motions seen by radar wind profilers, J. Appl. Meteorol., 33, 984–995, https://doi.org/10.1175/1520-0450(1994)033<0984:MVMSBR>2.0.CO;2 , 1994.

National Centers for Environmental Prediction/National Weather Service/NOAA/U.S. Department of Commerce. 2000. NCEP/DOE Reanalysis 2 (R2). Research Data Archive at the National Center for Atmospheric Research, Computational and Information Systems Laboratory. https://doi.org/10.5065/KVQZ-YJ93. Accessed 7 Jan 2019.

Peterson, V. L., and B. B. Balsley.: Clear air Doppler measurements of the vertical component of wind velocity in the troposphere and stratosphere. Geophys. Res. Lett., 6(12), 1979, Rao, P. B., A. R. Jain, P. Kishore, P. Balamuralidhar, S. H. Damle, and G. Viswanathan.: Indian MST radar 1. System description and sample vector wind measurements using ST mode, Radio Sci., 30, 1125–1138, https://doi.org/10.1029/95RS00787, 1995.

Rao, T.N, K. N. Uma, D. Narayana Rao, and S. Fukao.: Understanding the transportation process of tropospheric air entering the stratosphere from direct vertical air motion measurements over Gadanki and Kototabang, Geophys. Res. Lett., 35, L15805, https://doi.org/10.1029/2008GL034220, 2008.

Rao, T. N., Uma, K. N, T. M. Satyanarayana and D. N. Rao.: Differences in Draft Core Statistics from the Wet to Dry Spell over Gadanki, India (13.5°N, 79.2°E), Mon.Wea.Rev, 137, 4293-4306, https://doi.org/10.1175/2009MWR3057.1, 2009.

Rao, V., D. Rao, M. V. Ratnam, K. Mohan, and S. Rao.: Mean Vertical Velocities Measured by Indian MST Radar and Comparison with Indirectly Computed Values, J. App. Meteo, 42(4), 541-552, https://doi.org/10.1175/1520-0450(2003)042<0541:MVVMBI>2.0.CO;2, 2003.

Stepanyuk, O., R. Jouni, V. Sinclair, Heikki, , Järvinen.: Factors affecting atmospheric vertical motions as analyzed with a generalized omega equation and the OpenIFS model. Tellus., 69. 1271563. https://doi.org/10.1080/16000870.2016.1271563, 2017.

Schumann, U., : The horizontal spectrum of vertical velocities near the tropopausefrom global to gravity wave scales. J. Atmos. Sci., 76, 3847-3862, https://doi.org/10.1175/JAS-D-19-0160.1, 2019

Tanaka, H. L., and A. Yatagai.: Comparative study of vertical motions in the global atmosphere evaluated by various kinematic schemes, J. Meteo.Soc.Jp., 78, 289-298, 2000.

Tiedtke., M.: A Comprehensive Mass Flux Scheme for Cumulus Parameterization in Large-Scale Models, Mon. Wea. Rev., 117 (8): 1779–1800, https://doi.org/10.1175/1520-0493(1989)117<1779:ACMFSF>2.0.CO;2, 1989.

Uma, K. N., and Rao, T. N.: Characteristics of Vertical Velocity Cores in Different Convective Systems Observed over Gadanki, India, Mon.Wea.Rev., 137, 954-974, https://doi.org/10.1175/2008MWR2677.1, 2009a.

Uma, K. N., and Rao, T. N.: Diurnal variation in vertical air motion over a tropical station, Gadanki ($13.5^{o}$N, $79.2^{o}$E), and its effect on the estimation of mean vertical air motion, J. Geophys. Res., 114, D20106, https://doi.org/10.1029/2009JD012560, 2009b.

Uma, K. N., Kumar, K. K., Das, S.S., Rao, T. N., and Satyanarayana, T. M.: On the Vertical Distribution of Mean Vertical Velocities in the Convective Regions during the Wet and Dry Spells of the Monsoon over Gadanki, Mon. Weather Rev., 140, 398–410, https://doi.org/10.1175/MWR-D-11-00044.1, 2011.

Yamamoto, M. K., N. Nishi, T Horinouchi, M Niwano, and S Fukao.: Vertical wind observation in the tropical upper troposphere by VHF wind profiler: A case study, Rad, Sci., 42, RS3005, https://doi.org/10.1029/2006RS003538, 2007.

**Figure captions**

**Figure 1.** Topographical maps of the (a) Gadanki MST radar, and (b) Kototabang EAR sites in MSL, generated by using the Shuttle Radar Topography Mission (SRTM) data (*Farr et al.*, 2007). Dots in the map indicate the radar locations.

**Figure 2.** Intercomparision of layer averaged daily *w* (12 UTC) measured from MST Radar with different reanalyses (ERAi, ERA5, MERRA-2, NCEP/DOE-2, and JRA-55) (12 UTC) over Gadanki for (a) January 2007, and (b) August 2007.

**Figure 3.** Same as Fig.2, but for Kototabang. Please note that for Kototabang, *w* is diurnal mean (24 hrs mean) for both EAR and reanalyses for (a) January 2008, and (b)August 2008.

**Figure 4.** Climatological monthly mean altitude profile of *w* obtained from MST Radar and 5-reanalysis over Gadanki. Horizontal lines indicate the standard error.

**Figure 5.** Same as Fig.4, but over Kototabang.

**Figure 6.** Monthly mean *w* obtained from (a) MST Radar and (b) ERAi for 5 years interval (from top to bottom) over Gadanki (12 GMT).

**Figure 7.** Same as Fig.6 but for diurnal mean over Kototabang.

**Figure 8.** Height profile of *w* at 12 GMT and diurnal mean (with 1 hour resolution) over Gadanki extracted from ERA5 (highest available time resolution).

**Figure 9.** Same as Fig.8 but for Kototabang.

**Figure10.** Comparison of relative differences in *w* between the reanalysis for Gadanki. Individual month differences are estimated and then averaged for each month.

**Figure 11.** Same as Fig.10, but for Kototabang.

**Figure 12.** (a) Map for spatial averaging (grid resolution), and height profiles of *w* for different spatial averaging at 00, 06, 12, and 18 UTC respectively.

**Figure 13.** Comparison of directional tendency of *w* between the radars and various reanalysis data sets for (a) Gadanki and (b) Kototabang. Updrafts are shown in top and third panels and downdrafts are shown in middle and bottom panels (for details see text).

**Figure S1 :** Monthly mean climatology of *w* obtained from (a) radars, (b) ERAi, (c) ERA5, (d) MERRA-2, (e) NCEP/DOE-2, and JRA-55 over Gadanki (left) and Kototabang (right). Gadanki data are at 12 UTC and Kototabang data are diurnal mean.

## Table captions

**Table 1.** The radar specifications and parameters used for the present measurements.

**Table 2.** Schemes of different reanalyses data used in the present study.

**Figure 1.** Topographical maps of the (a) Gadanki MST radar, and (b) Kototabang EA radar sites in MSL, generated by using the Shuttle Radar Topography Mission (SRTM) data (*Farr et al.*, 2007). Dots in the map indicate the radar locations.

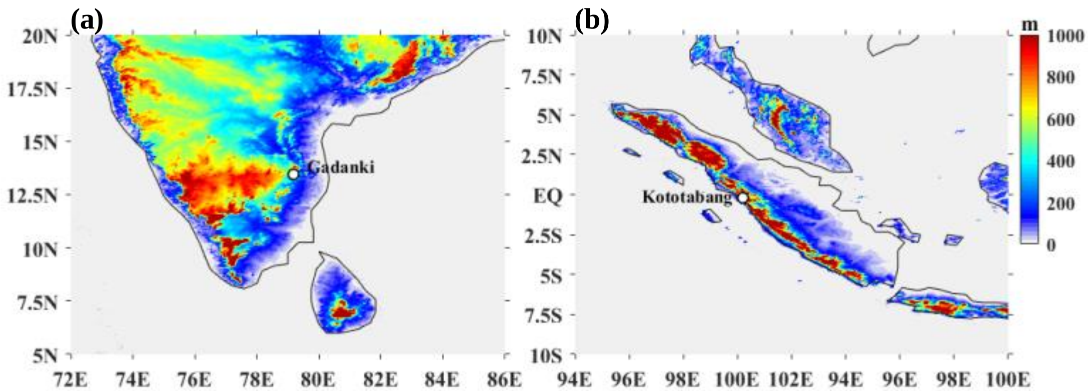

**Figure 2.** Intercomparision of layer averaged daily *w* (12 UTC) measured from MST Radar with different reanalyses (ERAi, ERA5, MERRA-2, NCEP/DOE-2, and JRA-55) (12 UTC) over Gadanki for (a) January 2007, and (b) August 2007.

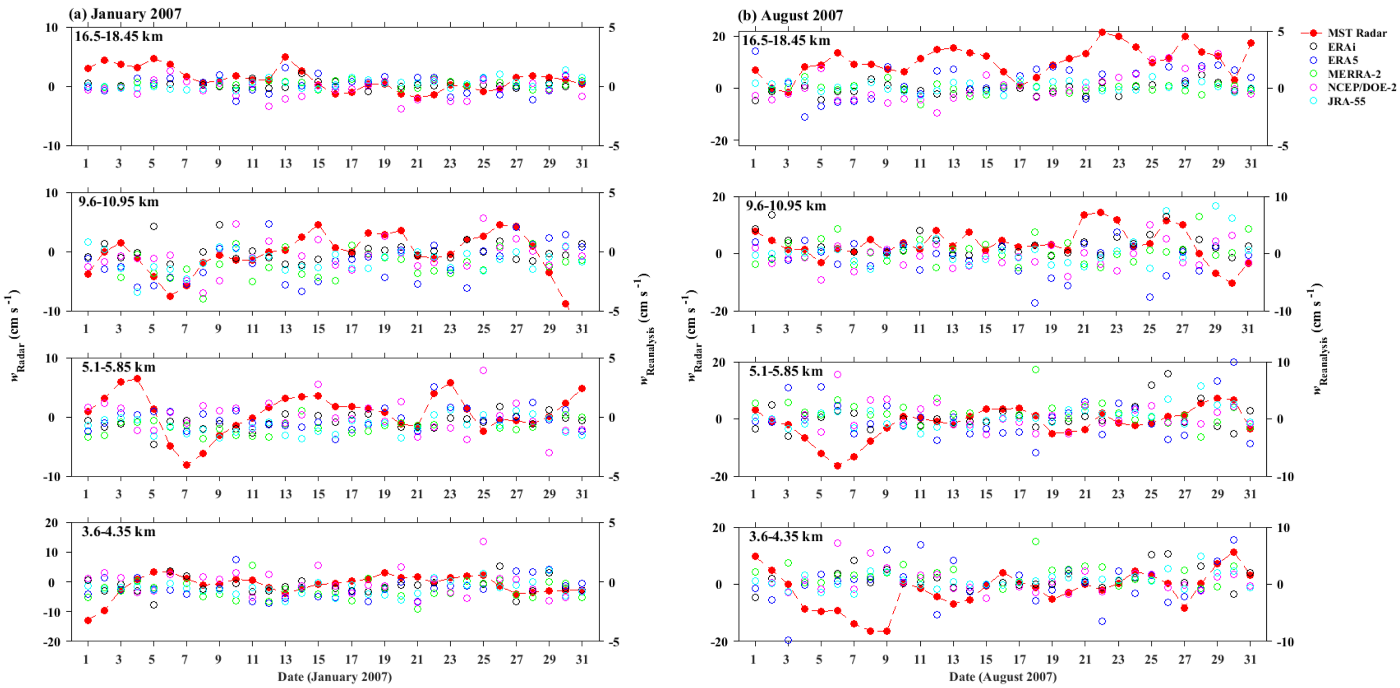

**Figure 3.** Same as Fig.2, but for Kototabang. Please note that for Kototabang, *w* is diurnal mean (24 hrs mean) for both EA radar and reanalyses for (a) January 2008, and (b) August 2008.

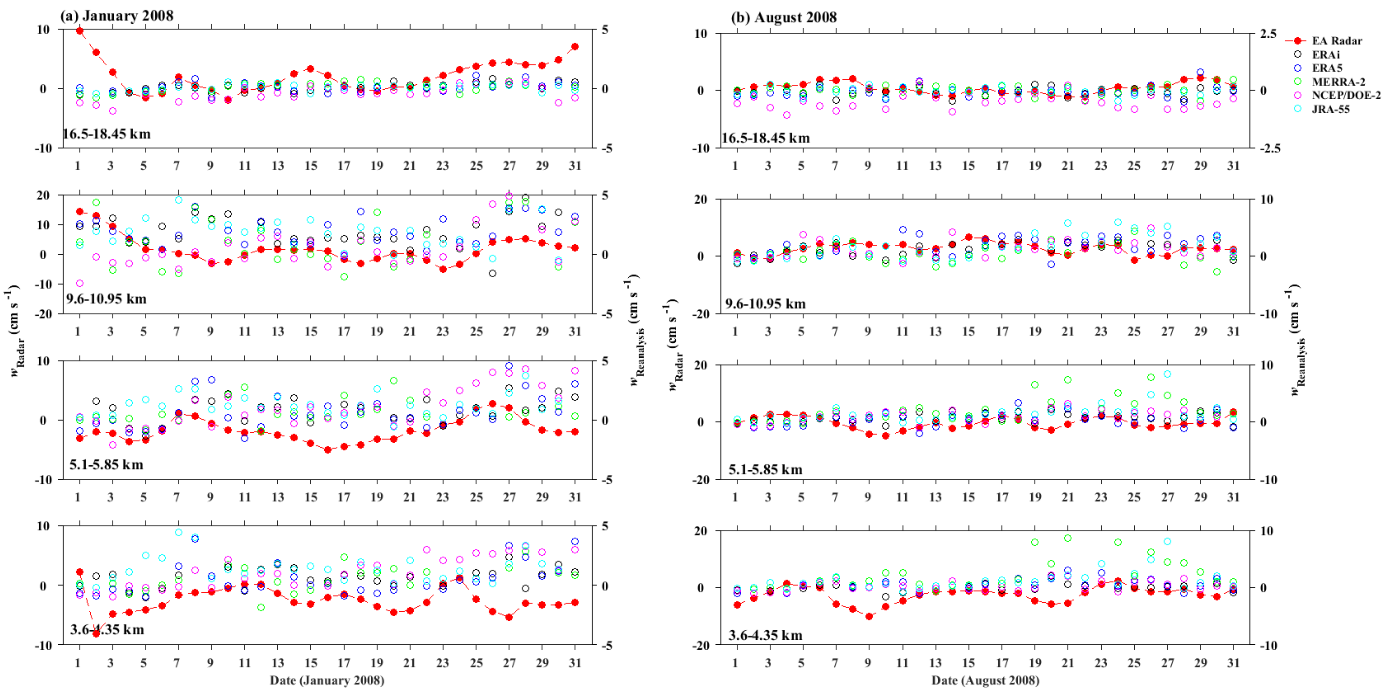

**Figure 4.** Climatological monthly mean altitude profile of *w* obtained from MST Radar and 5-reanalysis over Gadanki. Horizontal lines indicate the standard error.

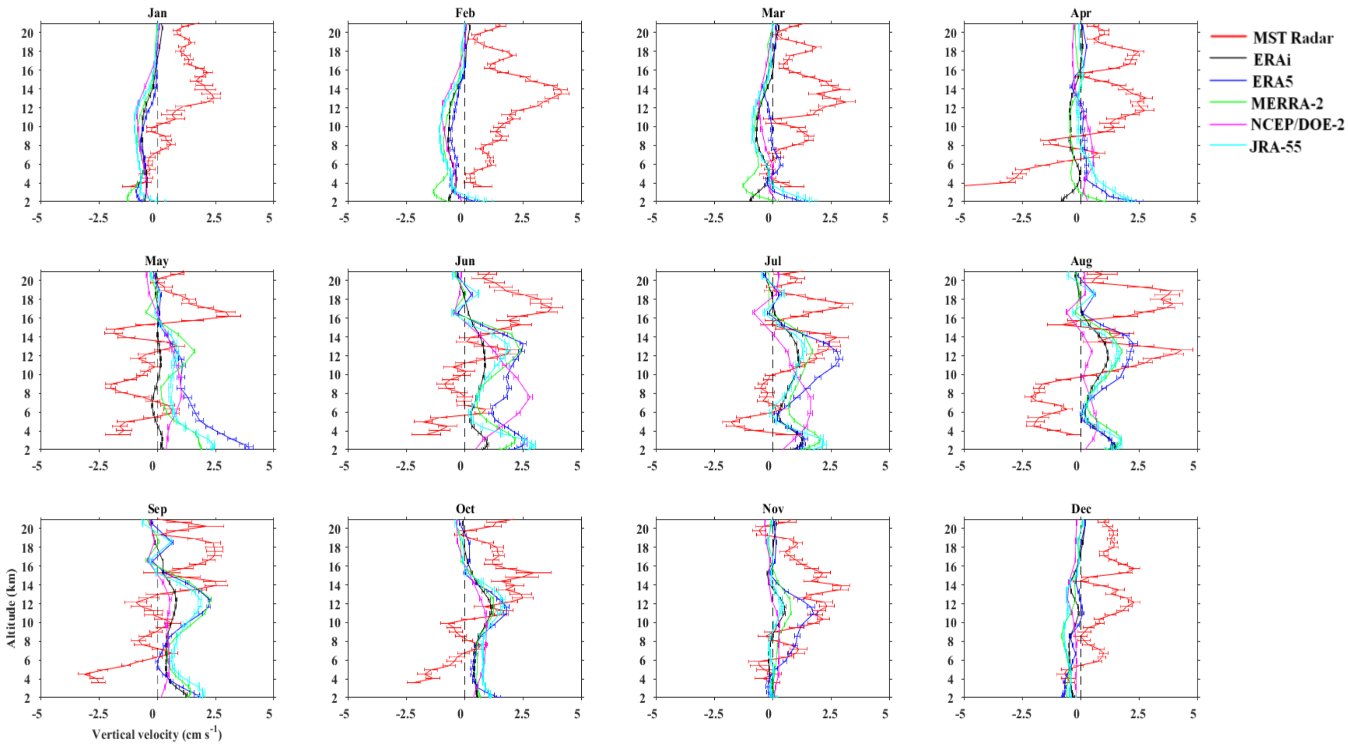

**Figure 5.** Same as Fig.4, but over Kototabang.

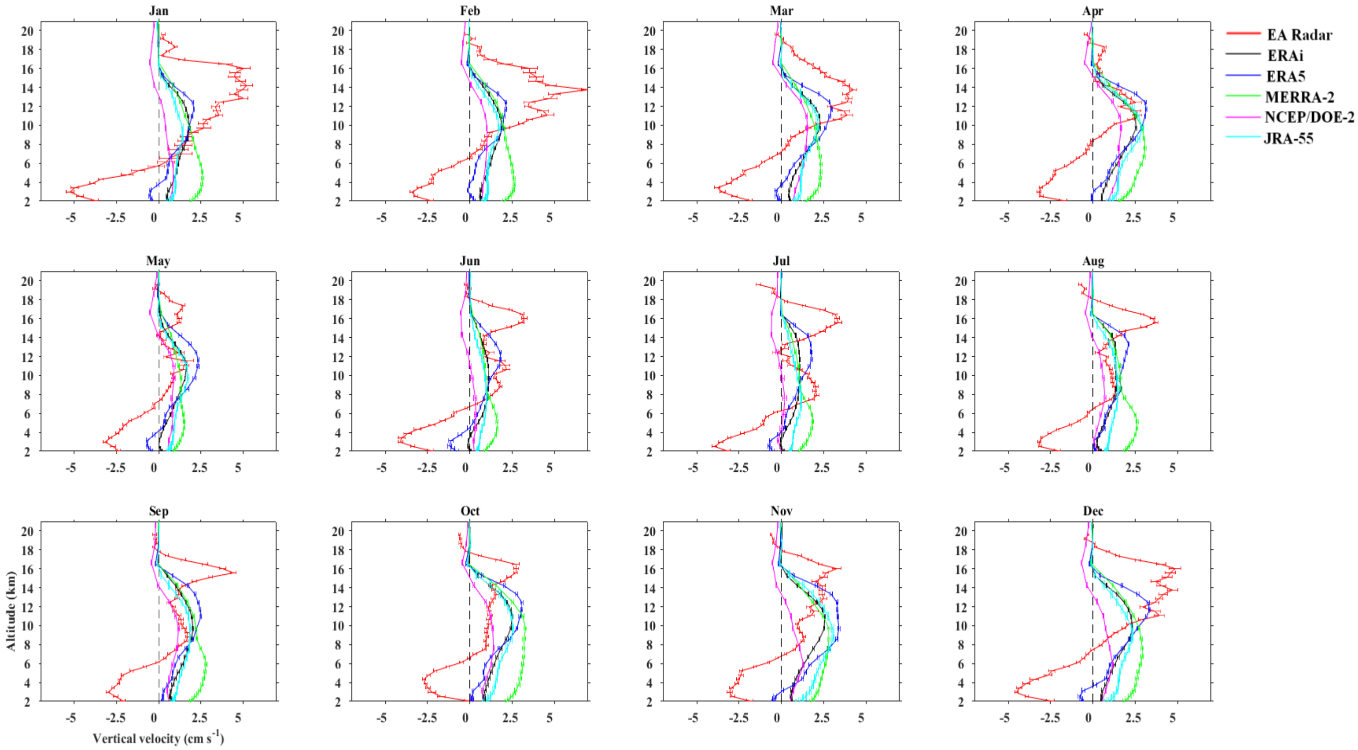

**Figure 6.** Monthly mean *w* obtained from (a) MST Radar and (b) ERAi for 5 years interval (from top to bottom) over Gadanki (12 GMT).

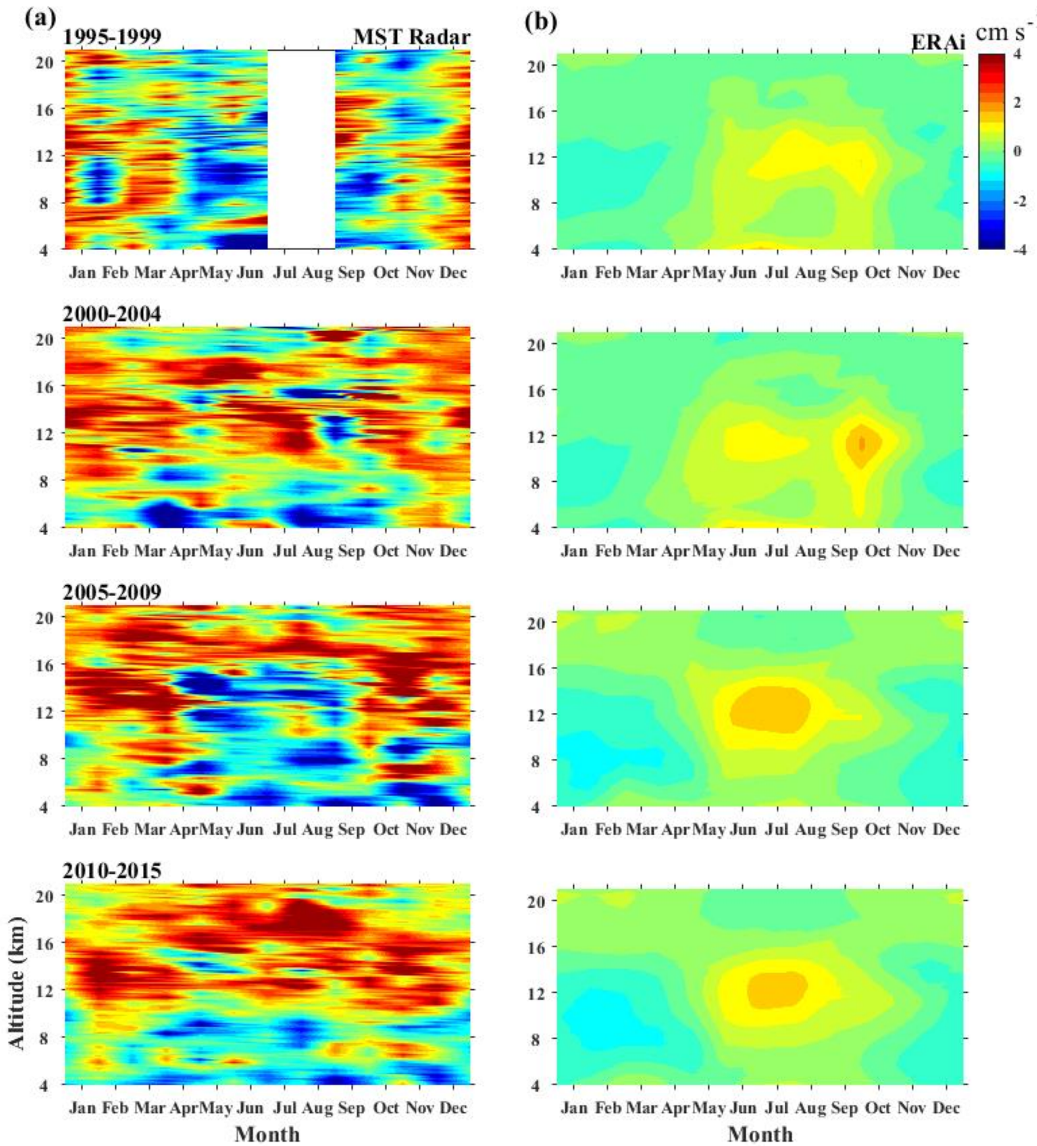

**Figure 7.** Same as Fig.6 but for diurnal mean over Kototabang.

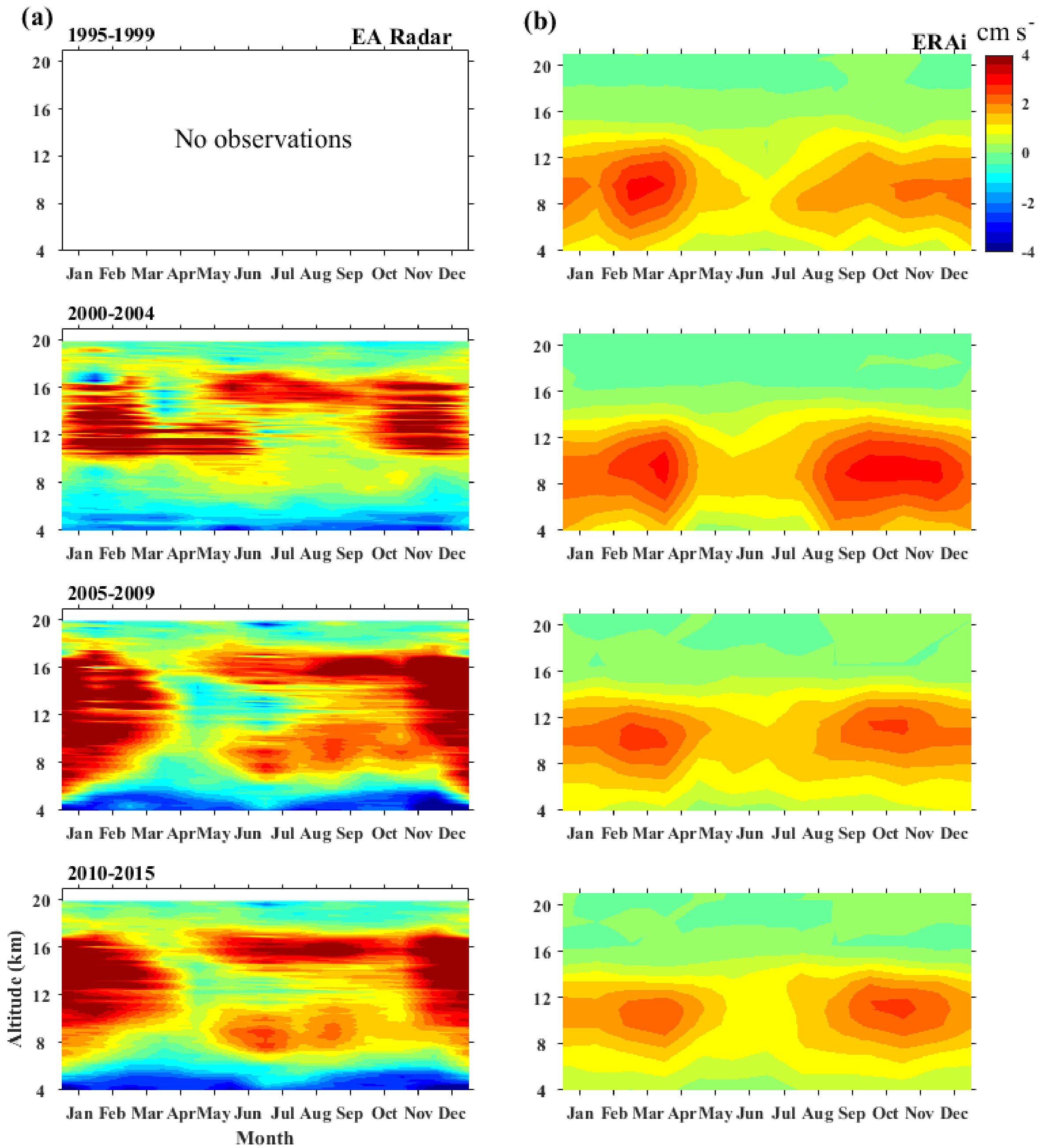

**Figure 8.** Height profile of *w* at 12 GMT and diurnal mean (with 1 hour resolution) over Gadanki extracted from ERA5 (highest available time resolution).

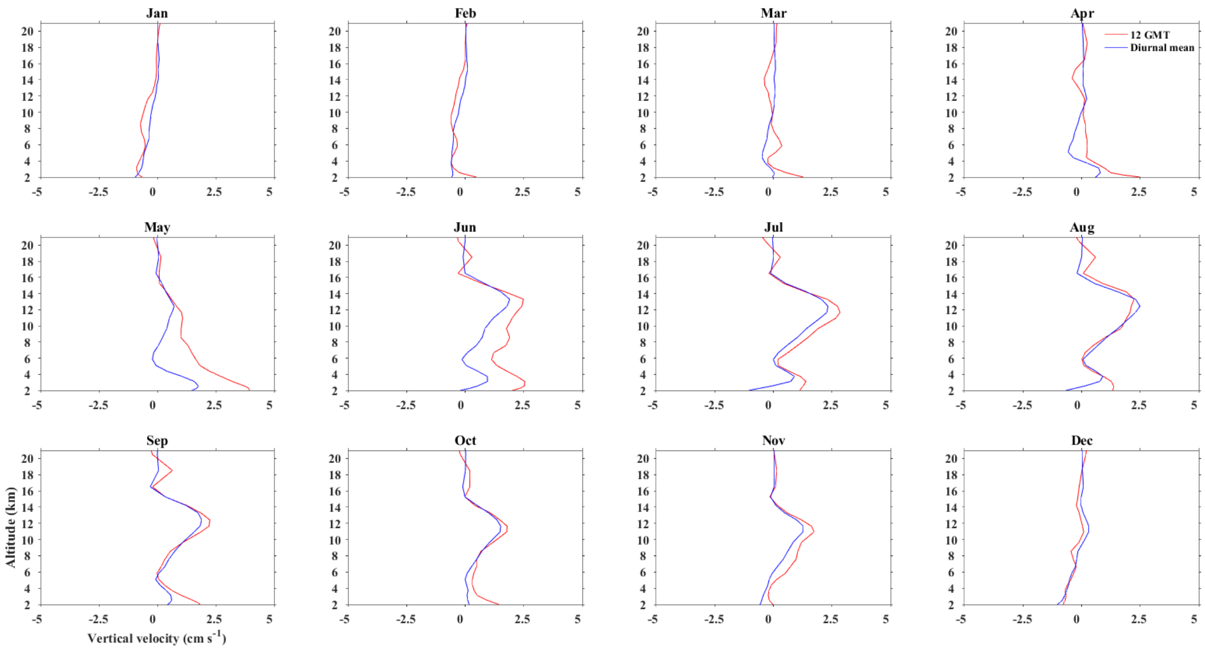

**Figure 9.** Same as Fig.8 but for Kototabang.

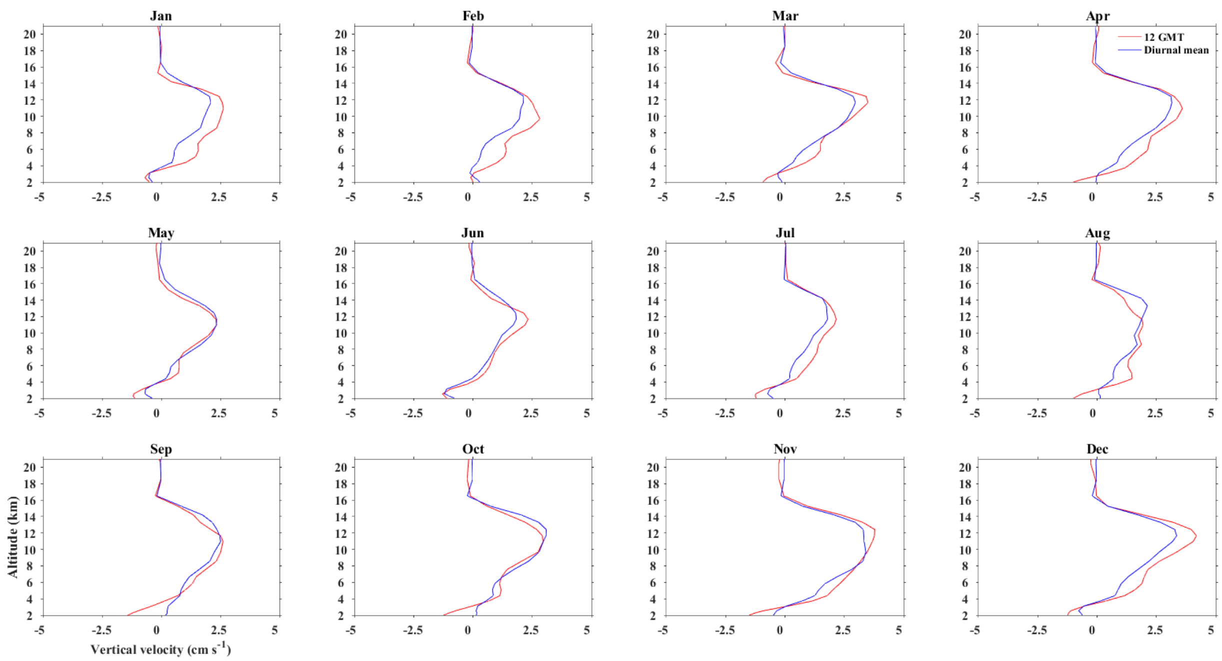

**Figure10.** Comparison of relative differences in *w* between the reanalysis for Gadanki. Individual month differences are estimated and then averaged for each month.

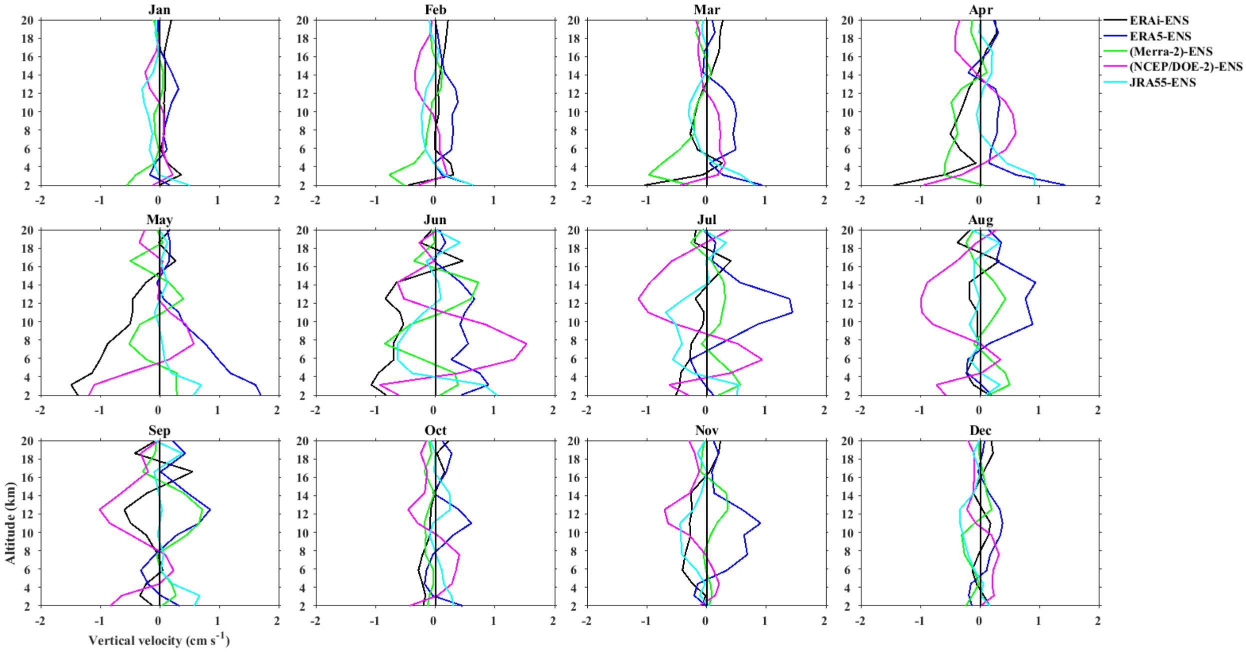

**Figure 11.** Same as Fig.10, but for Kototabang.

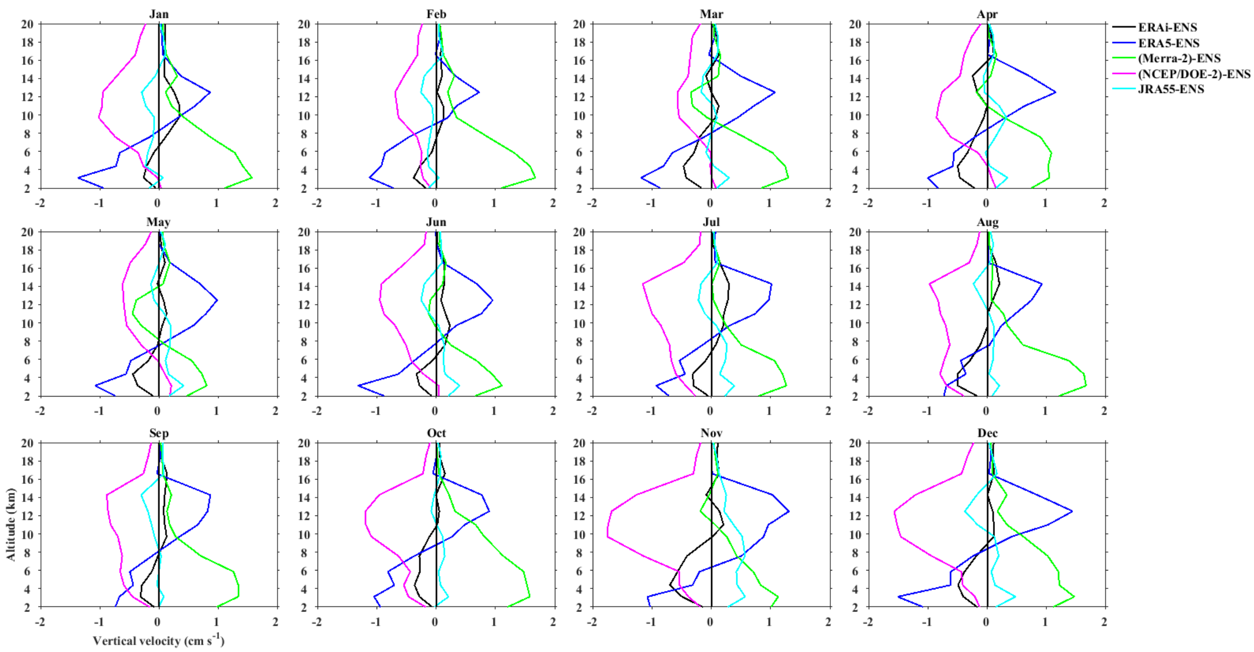

**Figure 12.** (a) Map for spatial averaging (grid resolution), and height profiles of *w* for different spatial averaging at 00, 06, 12, and 18 UTC respectively.

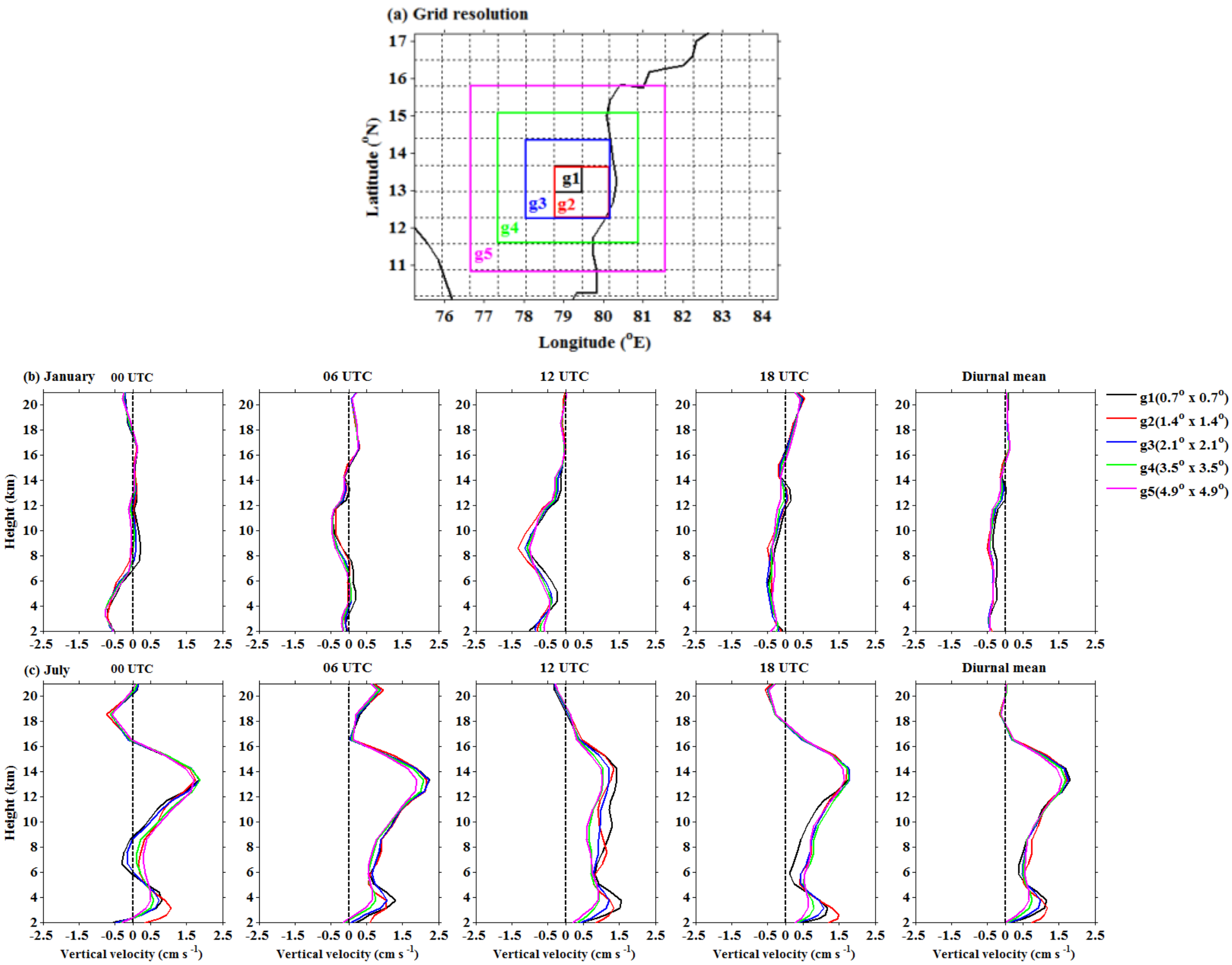

**Figure 13.** Comparison of directional tendency of *w* between the radars and various reanalysis data sets for (a) Gadanki and (b) Kototabang. Updrafts are shown in top and third panels and downdrafts are shown in middle and bottom panels (for details see text).

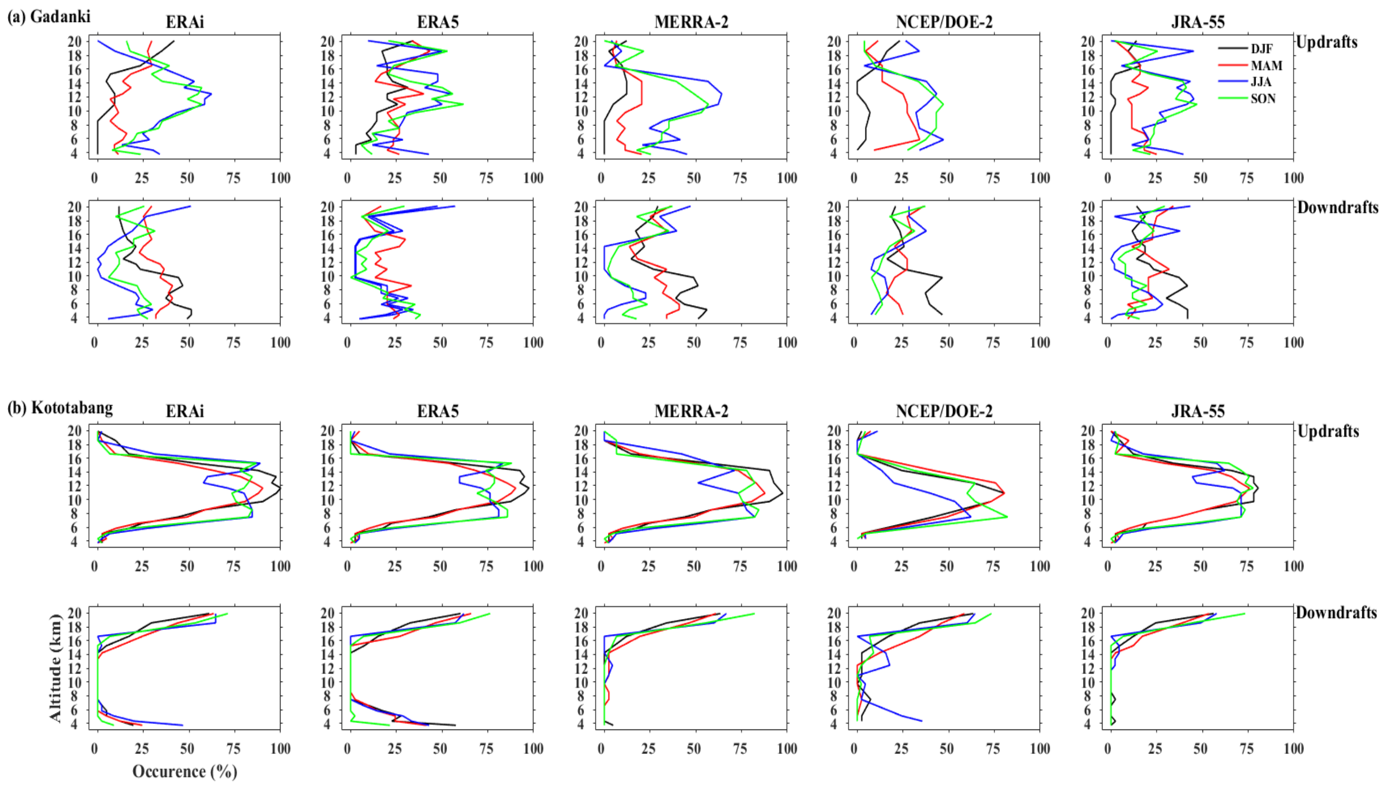

**Figure S1 :** Monthly mean climatology of *w* obtained from (a) radars, (b) ERAi, (c) ERA5, (d) MERRA-2, (e) NCEP/DOE-2, and JRA-55 over Gadanki (left) and Kototabang (right). Gadanki data are at 12 GMT and Kototabang data are diurnal mean.

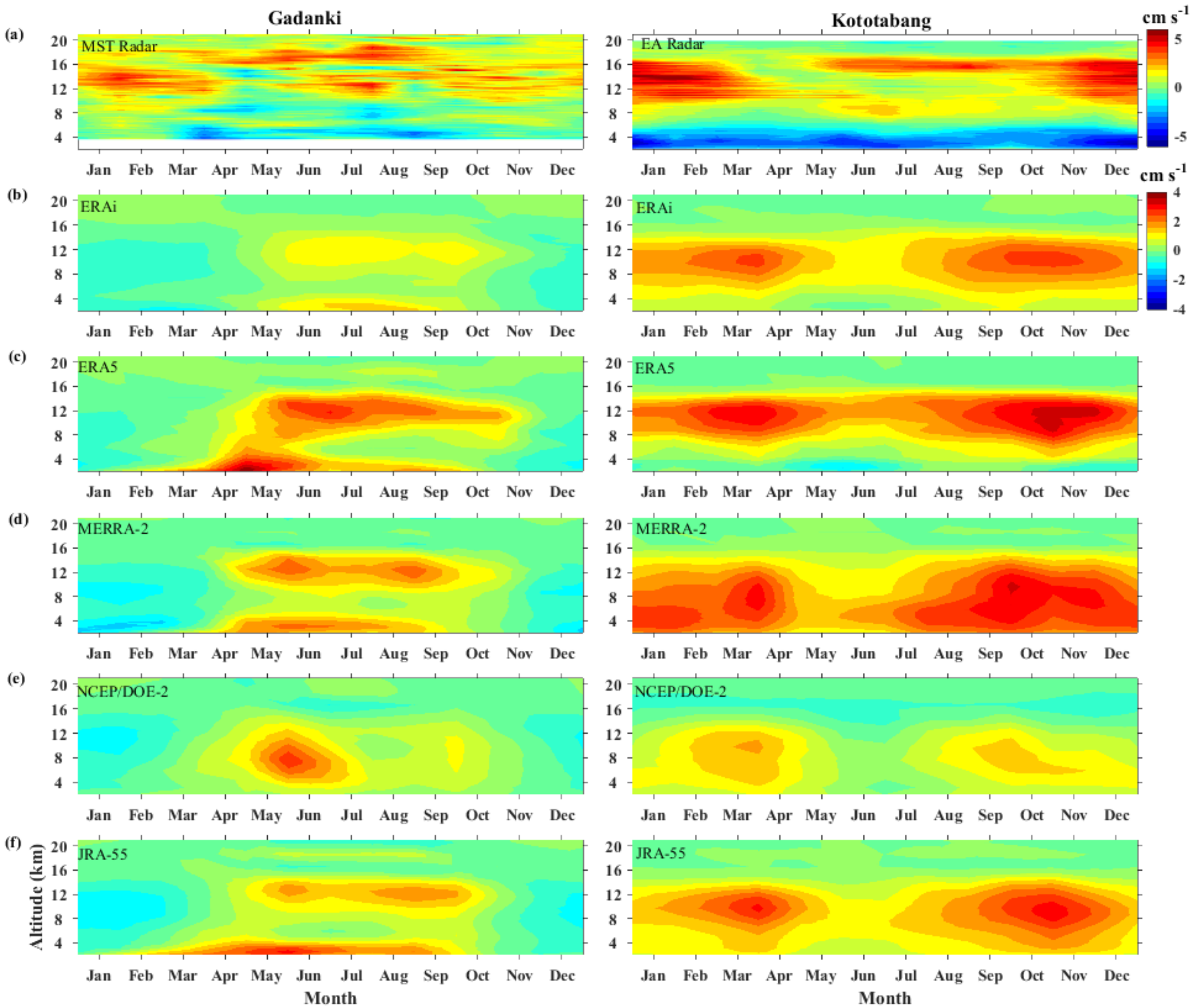

**Table 1.** The radars specifications and parameters used for the present measurements.

| **Parameter** | **IMSTR** | **EAR** |
|---|---|---|
| Frequency | 53 MHz | 47 MHz |
| Peak power | 2.5 MW | 100 kW |
| Maximum duty cycle | 2.5 % | 5 % |
| Antenna | 1024, three-element Yagi antennas | 560, three-element Yagi antennas |
| Beam width | 3 degree | 3.4 degree |
| Mode of operation | | |
| Pulse width | 16 $\mu$s with complimentary with 1 μs baud | 0.5 to 256 $\mu$s |
| Inter pulse period | 1000 $\mu$s | 200 and 400 $\mu$s |
| Range Resolution | 150 m | 150 m |
| No. of FFT point | 256 | 256, 512 |
| No of coherent integration | 64, 128, 256, and 512 | 16 and 32 |
| No. of Incoherent integration | 1 | 5 and 7 |
| No. of beam | 6 | 5 |
| | 10-degree off-zenith in East, West, North and South along with two orthogonal in zenith beams | 10-degree off-zenith in East, West, North and South along with one zenith beams |
| Data format | Spectrum | Spectrum |

**Table 2.** Schemes of different reanalyses data used in the present study.

| Description | ERA-Interim | ERA5 | MERRA2 | JRA55 | NCEP2 |
|---|---|---|---|---|---|
| Spatial Resolution | 0.75° x 0.75° | 0.28° x 0.28° | 0.5° x 0.65° | 1.25° x 1.25° | 2.5° x 2.5° |
| Longwave | *Mlawer et al.*, (1997) | *Morchrette*, (1991) | *Chou et al.*, (2001) | *Chou et al.*, (2001) | *Mlawer et al.*, (1997) |
| Shortwave | *Fouquart and Bonnel*, (1990) | *Iacono et al.*, (2008) | *Chou and Suarez*, (1999) | *Briegleb*,(1992) | *Chou.*, (1992); *Chou and Lee*, (1996) |
| Convective Parametrization | *Tiedtke*, (1989) | Convective mass flux scheme *Tidkete*, (1989) | Relaxed Arakawa-Schubert (RAS, *Moorthi and Suarez*, 1992) | Prognostic Arakawa-Schubert with DCAPE | Simplified *Arakawa Schubert scheme*, (1974) |
| Cloud Scheme | *Bechtold et al.*, (2004) | *Bechtold et al.*, (2008) | *Molod et al.*, (2015). | *Kawai and Inoue*, (2006) | *Campana et al.*, 1994 |
| Data Assimilation | 4D var | 4D var | 3D var with IAU | 4-D var | 3D VAR |
| References | *Dee et al.*, (2011) | *Hersbach et al.*, (2020) | *Gelaro et al.*, (2017) | *Kobayachi et al.*, (2015) | *Kanamitsu et al.*, (2002) |
| Vertical levels | L60 | L137 | L72 | L40 | L28 |